Air-stable Copolymer Exhibiting Near-Infrared Long-Persistent Luminescence

Zesen Lin[#]*, Maosheng Li*[#]*, Ryota Kabe**

Dr. Z. Lin, Prof. R. Kabe
Organic Optoelectronics Unit, Okinawa Institute of Science and Technology Graduate University
1919-1 Tancha, Onna-son, Okinawa, 904-0495, Japan
E-mail: ryota.kabe@oist.jp

Dr. M. Li
Key Laboratory of Polymer Ecomaterials, Changchun Institute of Applied Chemistry, Chinese Academy of Sciences
5625 Renmin Street, Changchun, 130022, P.R. China

# These authors contributed equally to this work.

Keywords: organic long persistent luminescence, near-infrared, copolymer

Abstract: Organic materials exhibiting long-lasting emission in the near infrared are expected to have applications in bio-imaging and other areas. Although room temperature phosphorescence and thermally activated delayed fluorescence display long-lived emission of approximately one minute, organic long-persistent luminescence (OLPL) systems with a similar emission mechanism to inorganic persistent emitters can emit for several hours at room temperature. In particular, OLPL with a hole-diffusion mechanism can function even in the presence of oxygen. However, ionic materials lack long-term stability in neutral organic host owing to aggregation and phase separation. In this study, we synthesised polymers with stable near-infrared persistent luminescence at room temperature via the copolymerisation of electron donors and acceptors. The copolymers exhibit long-persistent luminescence (LPL) at temperatures below the glass transition temperature and can be excited by approximately the entire range of visible light. LPL properties and spectra can be controlled by the dopant.

1. Introduction

Organic materials that display near-infrared (NIR, 700–2,500 nm) persistent emission at room temperature have attracted attention because of their applications in biological imaging[1-4], biosensing[5], photodynamic therapy[6], and cancer theragnostics[7]. The long-lived room-temperature emission of organic materials can be subdivided into: room-temperature phosphorescence (RTP)[8-11], thermally activated delayed fluorescence (TADF)[3, 12], and long-persistent luminescence (LPL)[13, 14]. The duration of RTP and TADF is generally shorter than one minute, because these systems store energy in the triplet excited state and cannot store energy for long periods because of competing non-radiative deactivation.[15] By contrast, LPL is caused by the gradual recombination of trapped electrons and holes and can extend to photoluminescence that is hours-long because holes and electrons are stable unless recombined. LPL that follows power-law decay can be clearly distinguished from RTP and TADF by following exponential decay which is widely observed in organic materials.[14, 16-18] In inorganic LPL research, the power-law afterglow is referred to as persistent luminescence, by consensus of opinion.[14, 18, 19] Inorganic LPL materials that exhibit NIR emission have potential for biological applications, but their application is restricted by size limitations and the toxicity of heavy metals.[15, 20]

Organic LPL (OLPL) systems store energy as charge carriers, similar to inorganic LPL materials.[13, 21-30] Basic OLPL systems comprise electron donors and electron acceptors and generate charge carriers via photo-induced charge separation between the donor and acceptor interface. After charge separation, as occurs in organic solar cells, the generated donor radical cations and acceptor radical anions accumulate in the materials. According to the carrier diffusion mechanism, OLPL systems can be categorised as electron diffusion (n-type)[13, 21, 23, 24] or hole-diffusion (p-type)[26] types. Electrons diffuse through the acceptor material after charge separation when a small amount of electron donor and an excess of electron acceptor materials are mixed (**Fig. 1a**). By contrast, holes diffuse through the donor materials when electron donor materials are in excess. The charge recombination process is probabilistic and the rate-determining step in luminescence, thereby leading to power-law LPL emission.

The highest occupied molecular orbital (HOMO) of the donor and the lowest unoccupied molecular orbital (LUMO) of the acceptor are important in OLPL material design, because the HOMO-LUMO gap dominates the emission colour and contributes to the stability of the charge-separated states. After charge separation, holes are present in the donor HOMO and electrons are present in the acceptor LUMO. If the LUMO level occupied by one electron are higher than the redox potential of oxygen (−3.5 eV), quenching occurs due to electron transfer to oxygen. Therefore, p-type OLPL systems comprising shallow LUMO levels are more

https://doi.org/10.26434/chemrxiv-2023-t5bnk **ORCID:** https://orcid.org/0000-0002-3647-4262

oxygen-tolerant. Oxygen prevention is necessary to obtain high-efficiency LPL, because triplet excitons produced by charge recombination are quenched by energy transfer to oxygen.[26]

NIR-OLPL can be accomplished by reducing the HOMO-LUMO gap or adding NIR emitters to the OLPL system.[22, 26] The p-type NIR-OLPLs, that can function even under atmospheric conditions, are anticipated to be used in future bio-applications (Fig. 1b). However, high-polarity ionic dopants lack affinity with low-polarity neutral host materials. The thermodynamically unstable mixture results in long-term phase instability and reduced solvent resistance (Fig. 1c). The affinity problem of multiple materials can be solved by copolymerisation.[31] Copolymers constructed by electron donors and acceptors have reported improved stability in organic semiconducting devices compared with blend of polymers or small molecules.[31-35]

In this study, we report NIR-OLPL copolymers that are constructed by linking a small amount of ionic acceptor (M2) with a large number of carbazole donors (M1) onto a polymethyl methacrylate (PMMA) main chain (Fig. 1b). The copolymer that has a low doping concentration possesses LPL in the wavelength range of 600–1000 nm, which can be detected an hour after excitation (~ 1 mW/cm^2) with a range of ultraviolet (UV) to visible wavelengths. The luminescence mechanism of the OLPL copolymer is systematically analysed using time-resolved spectroscopy. LPL can be observed even in air and at high temperatures. The LPL durations and wavelengths can be controlled by adding carrier-trapping dopants and emitter dopants. The thermodynamically stable NIR-OLPL of copolymers shows promise for applications in autofluorescence-free *in-vivo* bio-imaging.

2. Results

2.1. Design, synthesis, and basic physical properties of copolymers.

We developed donor-acceptor nonconjugated copolymers because charge separation does not require conjugation between the donor and acceptor units. The polymer was modified on a PMMA backbone with carbazole derivative (M1) as the donor and 2,4,6-*tris*(methoxyphenyl)pyrylium (MeOTPP$^+$) derivative (M2) as the acceptor. The copolymers were based on poly(2-(9H-carbazol-9-yl)ethyl methacrylate) (PMCz), which is deemed suitable as a host matrix in myriad photoelectronic applications[34-38]. The PMMA backbone provides a polar environment that enhances the affinity with ionic M2. To determine by the nuclear magnetic resonance (NMR) that M2 underwent copolymerisation, we used acrylic ester instead of methyl acrylic ester in M2.

4-(4-(Acryloyloxy)phenyl)-2,6-*bis*(4-methoxyphenyl)pyrylium tetrafluoroborate (M2) was synthesised via a condensation reaction (**Supplementary Scheme 1**). PMCz and copolymers (CP1–CP4) were prepared via free radical polymerisation of the corresponding 2-(9H-carbazol-9-yl)ethyl methacrylate (M1) and different amounts of M2 monomers using 2,2′-azo*bis*isobutyronitrile (AIBN) as the initiator and dimethylacetamide (DMAc) as the solvent (Fig. 1b; a detailed description of the synthesis is provided in Supplementary Information 3.3). The structures of PMCz and CP1–CP4 were confirmed by ^{1}H NMR and ^{1}H-^{1}H correlation spectroscopy (COSY) results (Supplementary Fig. 3–6). The multiple peaks at 1.75–2.25 ppm originate from the hydrogen atom of the acrylic double bond of the copolymers, thereby indicating the successful copolymerisation between M1 and M2. The newly observed broad peaks at 3.4–5.0 ppm and 6.6–9.3 ppm, which can be attributed to the methoxy and pyrylium protons derived from the pyrylium moieties present in the copolymer, provided indirect confirmation of the copolymerisation.

The ratio between M2 and M1 (m/n) and the weight fraction of M2 (ω (M2)) in the copolymers were calculated from the molar extinction coefficient of monomers and absorbance of copolymers (Fig. 2a; a detailed description of the calculations is provided in Supplementary Information 3.4). The fraction of the copolymer originating from M2 was negligible (m/n of CP1–CP4:0.003–0.009). Size exclusion chromatography (SEC) analysis revealed a gradual decrease in the average molecular weights (M_n) and polydispersity indices (PDI) of copolymers as the proportion of M2 in the copolymer increased (**Table 1**), thereby indicating that M2 functioned as a polymerisation inhibitor.

In terms of thermal properties, the thermal decomposition temperatures (T_d) of the copolymers exceed 270 °C, and the glass transition temperatures (T_g) fall within the range of 133–147 °C, emphasising their good thermal and morphological stability (Table 1, Supplementary Fig. 8). Given the absence of any discernible melting points below 250 °C, these copolymers are classified as amorphous thermoplastic materials.

The spatial separation of the donor and acceptor groups ensured that the redox properties of M1 and M2 remained essentially unaltered before and after polymerisation.[33] Therefore, we used the HOMO and LUMO energies of the monomers to represent those of the respective donor and acceptor moieties in the copolymer (Fig. 1b, Supplementary Fig. 9). The HOMO and LUMO levels of M2 were both 0.1 eV lower than those of MeOTPP$^+$ because a phenyl acrylate group replaced the 2-methoxyphenyl group. The HOMO of M1 was −5.5 eV, and is 0.2 eV lower than that of mCBP. The energy gap between the donor HOMO and acceptor LUMO of the copolymers was larger than that of the MeOTPP$^+$/mCBP system, thereby resulting in a red-shift of the CT emission.

2.2. Optical properties of copolymer films.

The absorption spectra of all the copolymers in DCM solution showed clear features of carbazole, M2, and weak CT above 550 nm (Fig. 2). All the copolymers (CP1–CP4) exhibited emission at approximately 550 nm, corresponding to M2 emission, and weak CT emission at approximately 800 nm in DCM solution. Copolymer solutions with low ω (M2) exhibited a more prominent CT emission compared with that of the solution of 1 wt% M2-doped PMCz (Fig. 2b); this result further supported successful copolymerisation. By contrast, because of the high CT probability in the solid state, all polymer films exhibited only CT emission at 690, 698, 714, and 732 nm with full widths at half maximum (FWHM) of 128, 122, 157, and 150 nm, respectively. The photoluminescence quantum yields (PLQY) of CP1–CP4 were 3.5%, 3.1%, 1.3%, and 0.7%, respectively. The emission spectra were redshifted as the acceptor M2 concentration increased. A similar trend was observed in the mixture of small molecules, such as MeOTPP/TPBi[26] and MeOTPP/mCBP (Supplementary Fig. 11a). The copolymers exhibited a larger spectrum red-shift than that of the M2/PMCz blend system, which had the same donor and acceptor concentrations. This effect indicated that the copolymers had a higher CT probability than that of the small-molecule/polymer blend because of the restricted donor-acceptor distance and uniform dispersion of the acceptor units.

After photoexcitation, copolymers CP1–CP3 exhibited LPL following power-law emission decay (Fig. 2d). CP1 and CP2 that had acceptor concentrations below 1 wt% yielded good LPL characteristics, whereas CP4 that had acceptor concentrations above 10 wt% almost quenched the LPL. This trend for the LPL was consistent with those of small-molecule systems.[13, 23, 26] Although the photoexcitation was not strong (365 nm, 1.42 mW, 1 min), the LPL intensity of CP2 remained above 0.1 $\mu W \cdot sr^{-1} \cdot m^{-2}$ at 10 min after excitation. Owing to the wavelength limitations of the spectroradiometer (380–780 nm) that was used (Supplementary Fig. 2a), the actual spectral radiance was approximately one-third larger than the value shown in Fig. 2d and Supplementary Fig. 11b. In contrast to the M2/PMCz blend system, the copolymers demonstrated a more prominent LPL (Supplementary Fig. 11b). This behaviour could be ascribed to the movement confinement of pyrylium moieties within the copolymer backbone, that led to a reduction in the charge recombination induced by molecular migration[39]. The LPL intensity and duration of the copolymers depended on the excitation power and duration (Supplementary Fig. 12) and was consistent with the general characteristics of LPL.

The copolymers could be excited by almost the whole range of visible light, even at 730 nm (Fig. 3). The relationship between the integrated LPL intensity and the excitation wavelength indicated that the optimal excitation wavelength was approximately 600 nm. This wavelength corresponded to the CT absorption band extending up to 750 nm; excitation of the CT band produced charge separation more efficiently than excitation of the donor or acceptor units. Strong absorption occurred at the film surface for excitation light up to 350 nm because of the excess donor units in the copolymers, and corresponded to donor absorption. Conversely, excitation light above 350 nm could reach the interior of the film. When the acceptor units or CT band was excited, the host remained transparent at the corresponding wavelength, allowing the excitation light to interact with a larger population of acceptor moieties or CT band without additional energy transfer processes. Owing to the negligible absorbance variation of the copolymer film within the 350–550 nm range, which corresponds to acceptor absorption, excitation within this range resulted in comparable LPL intensities and durations under equivalent photon flux conditions.

2.3. Emission mechanism of OLPL copolymer films.

The photo-induced charge separation of the copolymer films was confirmed by UV-vis-NIR absorption spectroscopy (Fig. 4). When charge separation occurred from the donor unit to the acceptor unit, carbazole radical cations and TPP radicals formed. The absorption spectra of the oxidised and reduced species were obtained from spectroelectrochemical measurements. The characteristic absorption peaks of the carbazole radical cation and TPP radical were located at 600–2500 nm and 500–600 nm, respectively. After UV excitation of the CP2 film, two absorption peaks were observed in the delta absorption spectrum, one at 600–2500 nm attributed to the carbazole radical cation and the other below 600 nm attributed to the TPP radical, thereby confirming the photo-induced charge separation in the CP2 film.

The OLPL system exhibited fluorescence, TADF, and phosphorescence, in addition to LPL, via charge separation. Emission decay profiles and spectra were obtained on time scales ranging from nanoseconds to thousands of seconds to analyse these multiple processes (Fig. 5). At 300 K, two exponential decays corresponding to fluorescence (in nanoseconds) and TADF (in microseconds), and a power-law decay corresponding to LPL were observed. The emission peak was located at approximately 690 nm and the spectra did not change with time, thereby confirming that all emission was from the single CT excited states (^{1}CT), and the influence of solid-state solvation effects was negligible in the copolymer[23, 40].

At 10 K, nanosecond exponential decay corresponding to fluorescence and a few hundred milliseconds exponential decay corresponding to phosphorescence were observed instead of the disappearance of TADF. This phosphorescence lifetime of CP2 was consistent with that of M2 (Supplementary Fig. 13b and 14). The emission peak was approximately 680 nm in all time regions, thereby suggesting that CT emission was the main emission, but the spectra changed over time. The spectral red-shift within 100 ns–10 µs originated from the emergence of ^{3}CT phosphorescence. On the millisecond to second scale, there was an increase in the 600 nm emission component, which corresponded to the local excited triplet state of the acceptor moieties (^{3}LE$_A$). Although a ^{3}CT energy level was sufficiently low compared with that of ^{3}LE$_A$, impeded charge transfer might allow simultaneous emission from ^{3}LE$_A$ and ^{3}CT. In the time region above 1s, the LPL became dominant, and an increased intensity above 700 nm was observed. This region corresponded to ^{3}CT, where ^{1}CT and ^{3}CT generated by charge recombination could be emitted simultaneously at low temperatures (Supplementary Fig. 15).

2.4. Thermal and air stability of LPL.

The LPL of the copolymer was clearly observed up to the glass transition temperature (T_g) (Fig. 6). The LPL signal was observed even at 400 K, thereby indicating the good thermal stability of the copolymer LPL. The decreasing trend of LPL from 200 K to 350 K was consistent with steady-state PL, thereby indicating that quenching was mainly a non-radiative transition in the emission process. By contrast, the LPL was strongly quenched above T_g, whereas the steady-state PL exhibited minimal quenching. This effect suggested that the enhanced mobility of the polymer chains above T_g expedited charge recombination. Accelerated fading of photo-induced radical cations of aromatic amines in polymers upon reaching T_g has also been reported previously[39].

The copolymer exhibited LPL even in ambient air (Fig. 6c, 6d). Although the LPL intensity weakened owing to the energy transfer to oxygen, sufficient LPL could be observed even after one day in ambient air. It was also possible to record approximately 1 min of NIR-LPL using a commercially available consumer digital camera (Fig. 6d).

2.5. LPL color adjustment

Further doping of the appropriate carrier traps and emitters can enhance the LPL performance and alter the emission colour.[22] In this study, we used DCM2 and IR780 as additional dopants (Fig. 7). The HOMOs of DCM2 and IR780 were shallower than those of the copolymers, allowing them to act as hole traps[26]. The addition of DCM2 did not change the LPL spectrum because there was little overlap between the DCM2 absorption and CP2 emission spectra. However, DCM2 could function as a hole-trap, thereby improving the LPL properties. When IR780 was added, LPL was obtained from IR780 via Förster energy transfer because of the large overlap between the absorption and CP2 emission peaks. The LPL of the IR780 doped system, located at 900 nm, was weaker than the actual LPL because of the lack of sensitivity of the detector and should be higher than that of CP2.

3. Discussion

In summary, we successfully designed and synthesised donor-acceptor copolymers exhibiting NIR-LPL in the range of 600-950 nm. Only copolymers with lower M2 ratios demonstrated prominent LPL behaviour. The copolymer CT absorption enabled excitation even at 730 nm. The direct excitation of the CT absorption band led to stronger LPL emission, and surpassed the performance achieved by exciting either the host or dopant independently. The charge separation process was confirmed by UV-vis-NIR spectroscopy. The emission mechanism of the copolymer was elucidated via time-resolved spectroscopy from nanoseconds to hundreds of seconds. The copolymer exhibited thermal stability, retaining a clear LPL up to T_g. Moreover, the copolymer exhibited LPL even in air. By doping NIR emitters acting as hole traps, we accomplished LPL emission at 800–1000 nm. These findings highlight the significant potential of OLPL copolymer systems for a range of applications, including but not limited to biological imaging and photodynamic therapy.

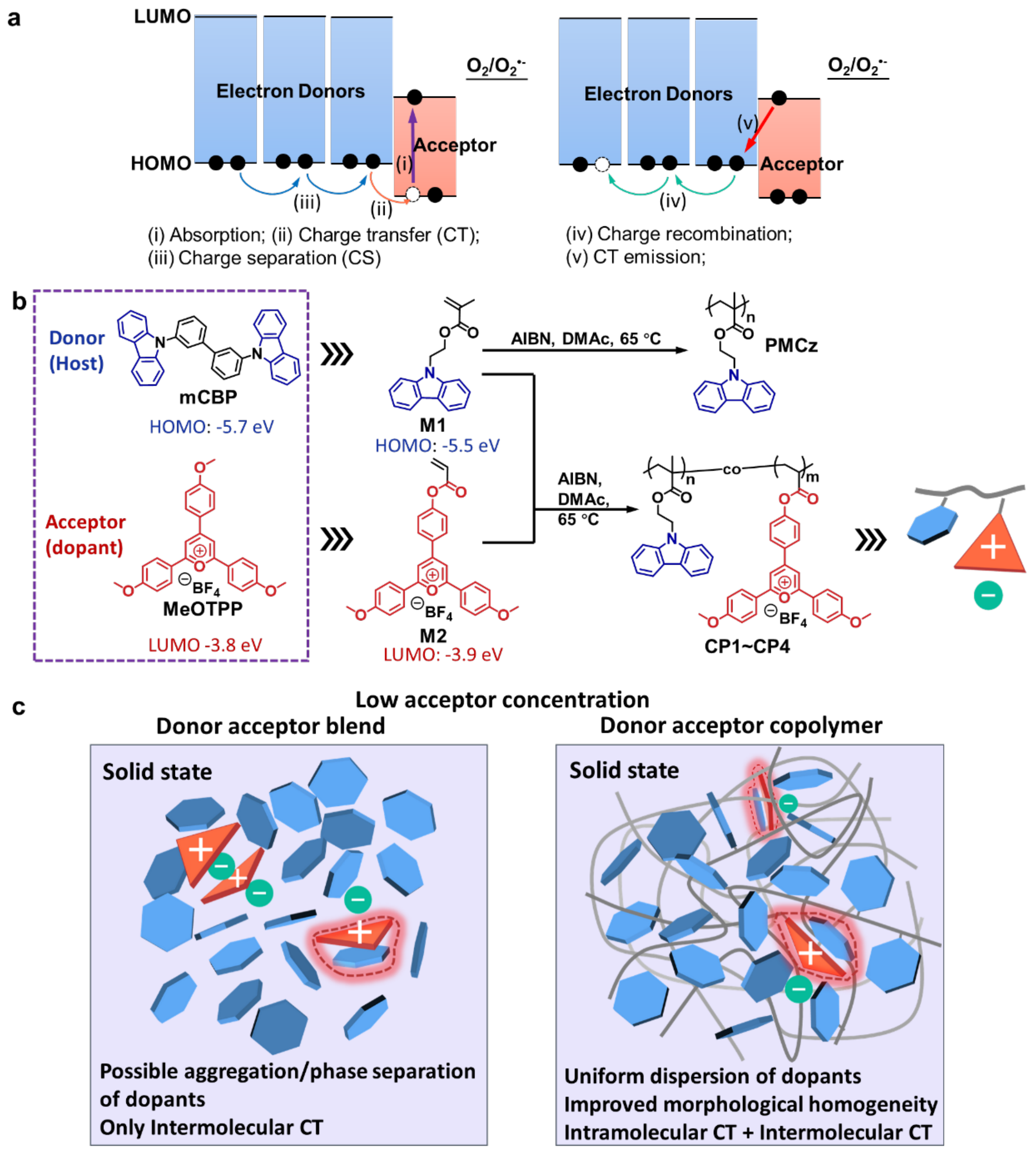

Fig. 1 │Emission mechanism and molecular design of OLPL systems. a, Emission mechanism of the p-type OLPL system in air. Charge separation occurs at the donor/acceptor interface. The charge-separated state is stabilised by the diffusion of holes through the donor HOMO. The charge recombination exhibits LPL from the acceptor LUMO to the donor HOMO. The electron transfer to the oxygen is prevented because the LUMO is deeper than the reduction potential of oxygen (−3.5 eV). **b**, Design and synthesis method of the NIR-OLPL copolymer. HOMO and LUMO levels of M1 and M2 were measured by cyclic voltammetry (CV). **c**, Schematic illustration of the advantages of the OLPL donor-acceptor copolymer with low acceptor concentrations. The red dashed line cycle represents the CT state.

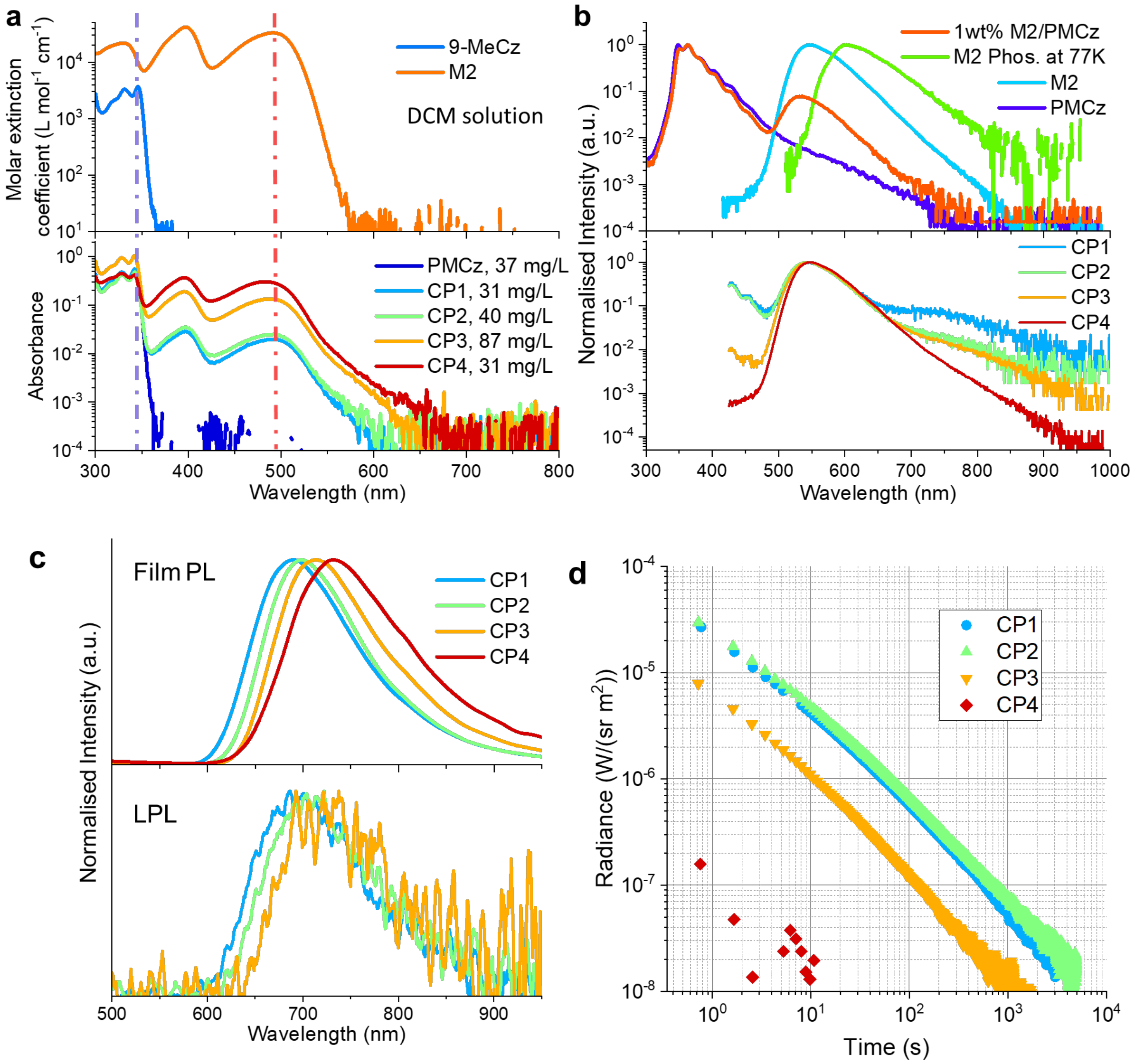

Fig. 2 │ Solution and film photophysical properties of OLPL copolymers. a, The UV-Vis absorption spectra of small molecules 9-MeCz and M2 (top), and polymers PMCz, CP1–CP4 (bottom) in DCM solution at room temperature. The purple and orange dashed lines represent the position of 343 nm and 490 nm, respectively. **b**, Steady-state photoluminescence (PL) of M2, PMCz, 1 wt% M2-doped PMCz (1 wt% M2/PMCz) in DCM at room temperature and the phosphorescence of M2 in DCM at 77 K (top). Steady-state PL of CP1–CP4 in DCM solution at room temperature (bottom). **c**, Steady-state PL spectra (top) and LPL spectra (bottom) of polymer films. **d**, Emission decay profiles of copolymers (CP1–CP4). Excitation condition of **c** and **d**: 365 nm, 1.4 mW/cm^2, 1 min, room temperature, under nitrogen gas.

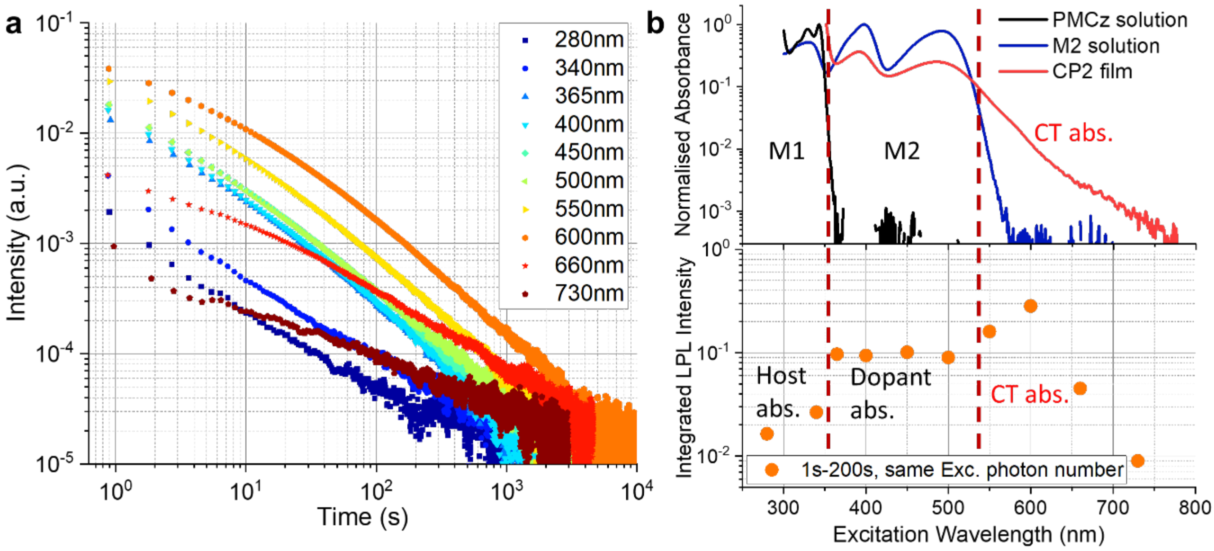

Fig. 3 │ Excitation wavelength dependence of LPL. a, LPL decay profiles of CP2 film excited by different wavelengths with the same excitation power and duration (1.0 mW/cm^2, 1 min) at room temperature. **b**, Absorption spectra of PMCz solution, M2 solution, and CP2 film (top). Integration emission intensity (1–200 s) vs. excitation wavelength at the same excitation photon numbers. The red dashed lines represent the demarcation between host, dopant, and CT absorption.

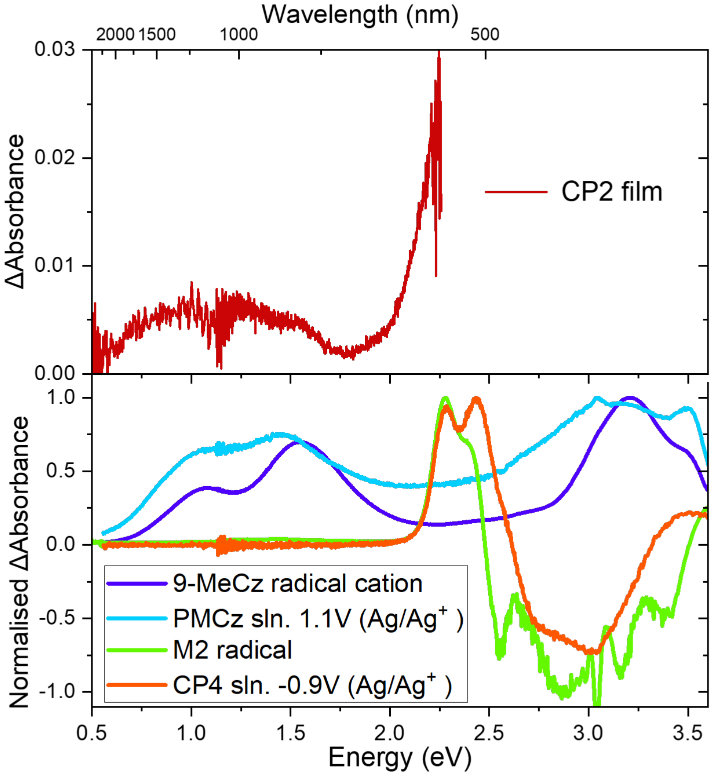

Fig. 4 │ Absorption spectra of charge-separated states and individual radicals. Top: Delta absorption spectra of CP2 film before and after photoexcitation at room temperature under nitrogen; **Bottom:** Delta absorption spectra of 9-MeCz, PMCz, M2 and CP4 in ACN that contains 0.1 M TBAPF$_6$ with and without electrical oxidation or reduction at 300 K under nitrogen.

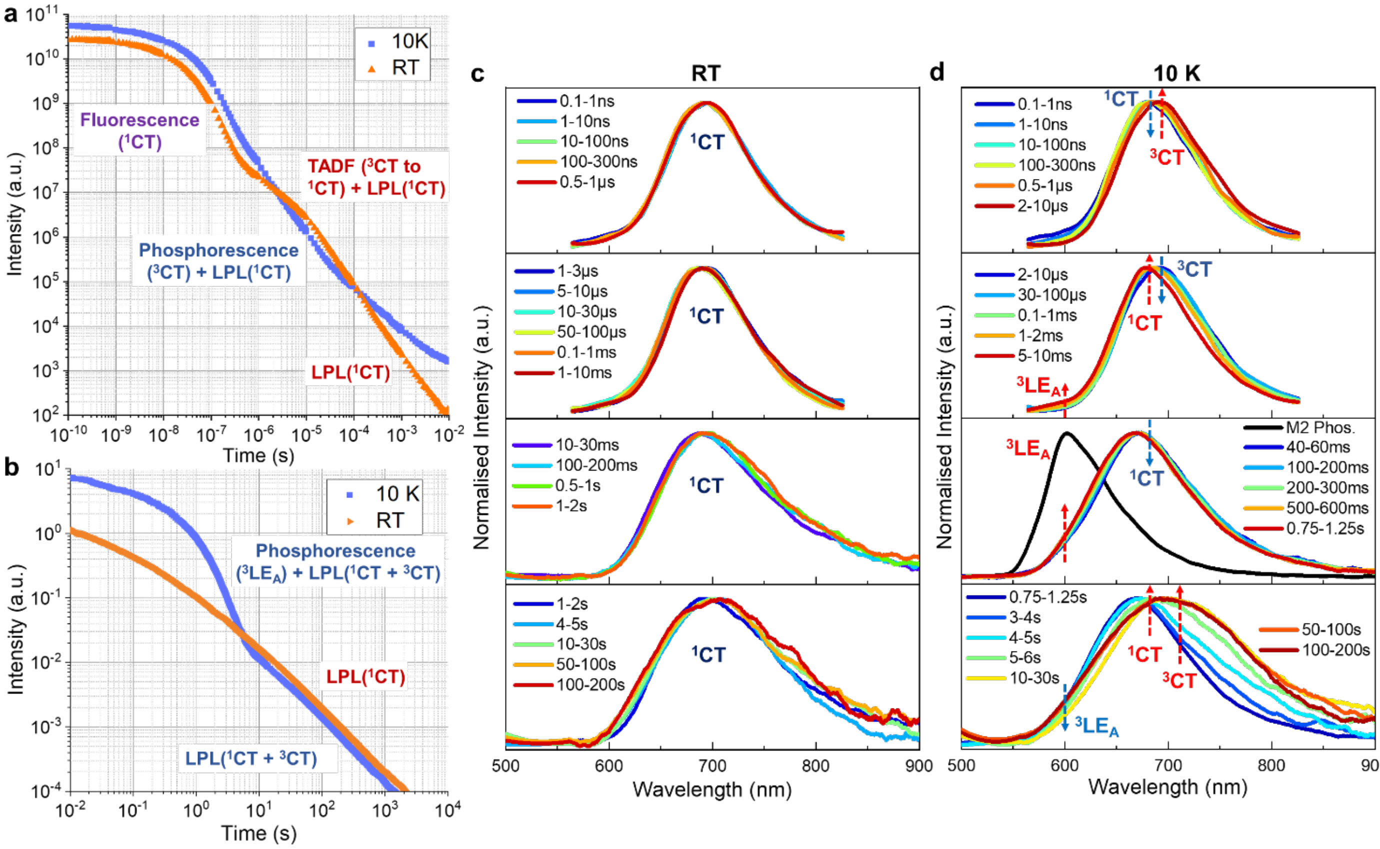

Fig. 5 │ Time-resolved emission decay profiles and spectra of copolymers.

a. Emission decay profiles of the copolymer film from 100 ps to 10 ms at 300 K and 10 K. Samples were excited by the pulsed laser (450 nm, 165 fs, 2 μJ, 25 Hz), and the emission intensity was obtained by the streak camera (integration 565-825 nm). **b.** Emission decay profiles of the copolymer film from 10 ms to 10^4 s at 300 K and 10 K. Samples were excited by LED (450 nm, 14.2 mW/cm^2, 1 min) and emission intensity was obtained by a multi-pixel photon counter. **c.** Time-resolved emission spectra of polymer film at 300 K. **d.** Time-resolved emission spectra of polymer film at 10 K. The spectra below 10 ms were obtained from the streak camera and above 10 ms by CCD. Because of the different excitation conditions and detectors, the two measurements do not perfectly match the spectra and decays.

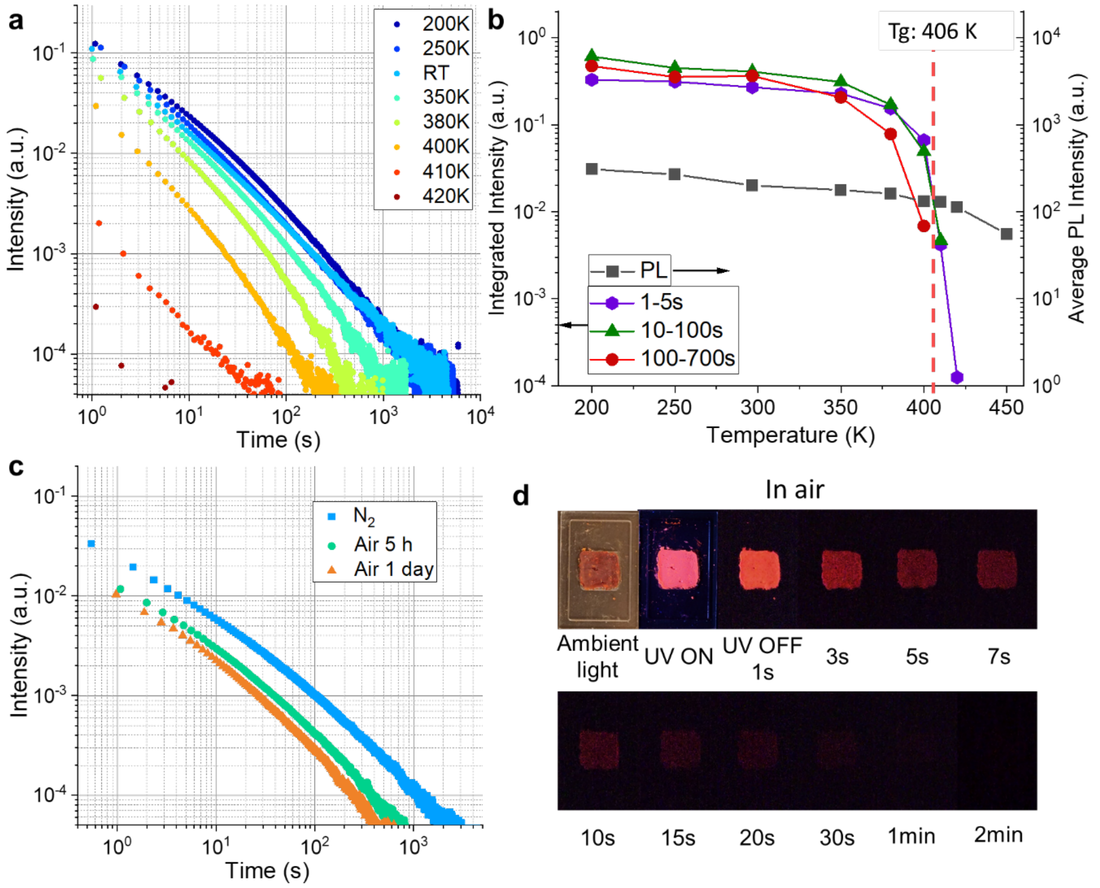

Fig. 6 │ LPL stability of copolymer under different conditions. a, LPL decay profiles of CP2 film at various temperatures (excitation: 450 nm, 14.2 mW/cm^2, 1 min). **b**, Integration LPL intensity (1–5 s, 10–100 s, 100–700 s) and steady-state PL intensity vs. temperature. The red dashed line represents the glass transition temperature. **c**, LPL decay profiles of CP2 film in nitrogen gas and air (excitation: 365 nm, 1.4 mW/cm^2, 1 min). Samples were stored in air for 5 hours or a day. **d**, Photographs of LPL emission of CP2 film at room temperature in air.

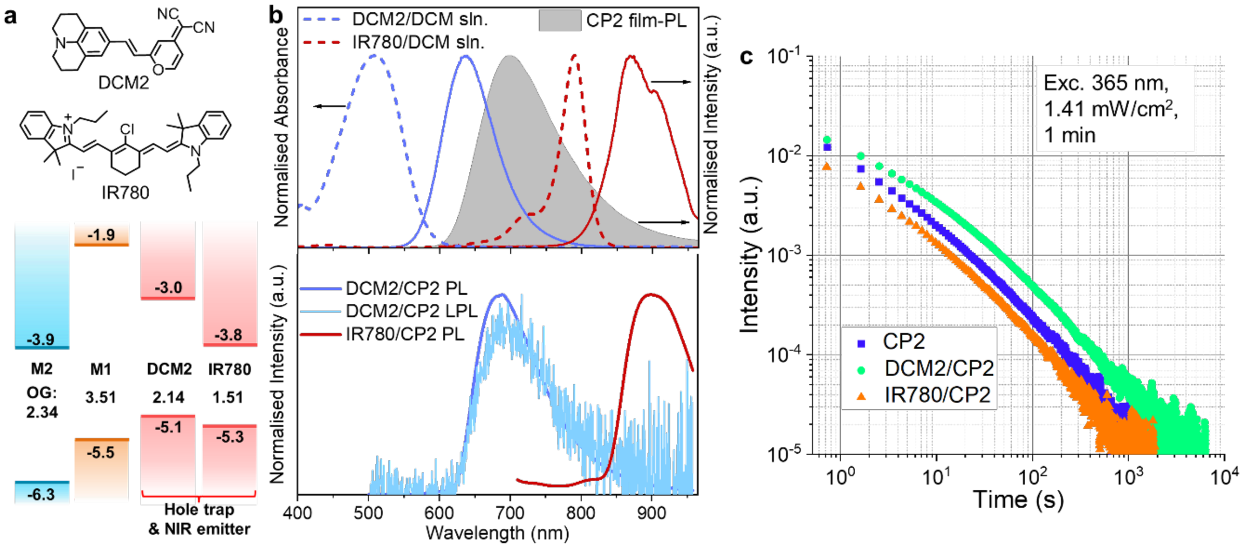

Fig. 7 │ Photoluminescence properties of copolymer with hole-trap dopant or emitter dopant. a, Chemical structures of NIR emitter dopants (DCM2 and IR780) and HOMO and LUMO levels and optical gaps (OG) of materials. HOMO and LUMO levels were obtained from electrochemical measurements and OGs were calculated from the absorption edge[22]. **b**, Top: Emission spectrum of the CP2 film and the absorption spectra of the emitter dopants in DCM solution. The dashed and solid line represent the absorption and fluorescence spectra, respectively, in solution. Bottom: Steady-state photoluminescence and LPL emission spectra of DCM2 or IR780 doped copolymer. Due to the weak sensitivity of the spectrometer, the LPL spectrum of the IR780 doped CP2 could not be obtained. **c**, LPL decay profiles of CP2 and DCM2 or IR780 doped copolymer (excitation: 365 nm, 1.4 mW/cm^2, 1 min).

Table 1. Characterisation of polymers

Polymer	Fraction of M2 (wt%)		m/n[a)]	M_n [b)]	PDI [b)]	T_g [c)]	T_d [d)]
	Monomer feed	In copolymer[a)]		[kg/mol]		[°C]	[°C]
PMCz	0.00	-	-	15.8	2.94	136	286
CP1	0.20	0.59	0.003:1	15.5	2.16	135	270
CP2	0.99	0.86	0.005:1	9.0	1.73	133	301
CP3	4.76	2.17	0.012:1	6.0	1.58	137	299
CP4	20.00	14.44	0.090:1	2.8	1.13	146	293

[a)] Calculated according to the molar extinction coefficient of monomers and absorbance of copolymers at 343 nm and 490 nm; [b)] Measured by SEC (THF, 35 °C), PS calibration; [c)] Glass transition temperatures (T_g) were measured using DSC under a N_2 atmosphere with a heating rate of 10 °C/min from room temperature to 250 °C (Supplementary Fig. 8b) [d)] Thermal decomposition temperatures (T_d) were measured by TGA at a heating rate of 20 °C/min in N_2 and determined at 5 % weight loss (Supplementary Fig. 8a).

Acknowledgements

This work was supported by the Japan Science and Technology Agency (JST) FOREST project (grant number JPMJFR201H); JSPS KAKENHI (grant number JP21H02020); the Jilin Science and Technology Bureau (Grant 20210402066GH, M.L.). We thank Prof. Youhua Tao in Changchun institute of applied chemistry, Chinese academy of sciences for his support and assistance in the synthesis experiments. We thank Prof. Kai Wang in Soochow University for sending the materials from China to Japan and Prof. Zhongbin Wu and Dr. Xiaobo Wang in Northwestern Polytechnical University for their help during the absorption spectroscopy tests of monomers. We thank K. Kusuhara and N. Nakamura for their assistance with the preparation of mCBP.

Zesen Lin and Maosheng Li contributed equally to this work.

Author contributions

Z.L. and R.K. designed this project. Z.L. designed the copolymer structure. Z.L. and M.L. designed synthesis route. M.L. carried out all synthesis, SEC, DSC, TGA experiments. Z.L. designed and carried out all other experiments. Z.L. and M.L. analysed data of synthesis part. Z.L. analysed all other data. R.K supervised the project. Z.L. and R.K. wrote the manuscript. All authors contributed to writing the paper and critically commented on the project.

References

1. Zhen X*, et al.* Ultralong Phosphorescence of Water-Soluble Organic Nanoparticles for In Vivo Afterglow Imaging. *Adv. Mater.* **29**, 1606665 (2017).

2. Fateminia SA, Mao Z, Xu S, Yang Z, Chi Z, Liu B. Organic Nanocrystals with Bright Red Persistent Room-Temperature Phosphorescence for Biological Applications. *Angew. Chem. Int. Ed.* **56**, 12160-12164 (2017).

3. Pan Y*, et al.* Highly Efficient TADF-Type Organic Afterglow of Long Emission Wavelengths. *Adv. Funct. Mater.* **32**, 2110207 (2022).

4. Dang Q*, et al.* Room-Temperature Phosphorescence Resonance Energy Transfer for Construction of Near-Infrared Afterglow Imaging Agents. *Adv. Mater.* **32**, 2006752 (2020).

5. Fan Y, Zhang F. A New Generation of NIR-II Probes: Lanthanide-Based Nanocrystals for Bioimaging and Biosensing. *Adv. Opt. Mater.* **7**, 1801417 (2019).

6. Li C*, et al.* Fluorination Enhances NIR-II Emission and Photothermal Conversion Efficiency of Phototheranostic Agents for Imaging-Guided Cancer Therapy. *Adv. Mater.* **35**, 2208229 (2023).

7. He S, Xie C, Jiang Y, Pu K. An Organic Afterglow Protheranostic Nanoassembly. *Adv. Mater.* **31**, 1902672 (2019).

8. Hirata S. Molecular physics of persistent room temperature phosphorescence and long-lived triplet excitons. *Appl. Phys. Rev.* **9**, 011304 (2022).

9. Chen C*, et al.* Carbazole isomers induce ultralong organic phosphorescence. *Nat. Mater.* **20**, 175-180 (2021).

10. Gu L*, et al.* Color-tunable ultralong organic room temperature phosphorescence from a multicomponent copolymer. *Nat. Commun.* **11**, 944 (2020).

11. Sk B, Tsuru R, Hayashi K, Hirata S. Selective Triplet–Singlet Förster-Resonance Energy Transfer for Bright Red Afterglow Emission. *Adv. Funct. Mater.* **33**, 2211604 (2023).

12. Xu Y*, et al.* Manipulation of Organic Afterglow in Fluoranthene-Containing Dopant-Matrix Systems: From Conventional Room-Temperature Phosphorescence to Efficient Red TADF-Type Organic Afterglow. *Chem. Eur. J.* **29**, e202203670 (2023).

13. Kabe R, Adachi C. Organic long persistent luminescence. *Nature* **550**, 384 (2017).

14. Xu J, Tanabe S. Persistent luminescence instead of phosphorescence: History, mechanism, and perspective. *J. Lumin.* **205**, 581-620 (2019).

15. Maldiney T*, et al.* The in vivo activation of persistent nanophosphors for optical imaging of vascularization, tumours and grafted cells. *Nat. Mater.* **13**, 418 (2014).

16. Randall JT, Wilkins MHF. Phosphorescence and electron traps II. The interpretation of long-period phosphorescence. *Proc. Math. Phys. Eng. Sci.* **184**, 390-407 (1945).

17. Era K, Shionoya S, Wasfflzawa Y, Ohmatsu H. Mechanism of broad-band luminescences in ZnS phosphors—II. Characteristics of pair emission type luminescences. *J. Phys. Chem. Solids* **29**, 1843-1857 (1968).

18. Smet PF, Van den Eeckhout K, De Clercq OQ, Poelman D. Chapter 274 - Persistent Phosphors. In: *Handbook on the Physics and Chemistry of Rare Earths* (eds Bünzli J-C, Pecharsky VK). Elsevier (2015).

19. Smet PF, Poelman D, Hehlen MP. Focus issue introduction: persistent phosphors. *Opt. Mater. Express* **2**, 452-454 (2012).

20. Viana B*, et al.* NIR-Persistent Luminescence Nanoparticles for Bioimaging, Principle and Perspectives. In: *Near Infrared-Emitting Nanoparticles for Biomedical Applications* (eds Benayas A, Hemmer E, Hong G, Jaque D). Springer International Publishing (2020).

21. Lin Z, Kabe R, Nishimura N, Jinnai K, Adachi C. Organic Long-Persistent Luminescence from a Flexible and Transparent Doped Polymer. *Adv. Mater.* **30**, 1803713 (2018).

22. Jinnai K, Kabe R, Adachi C. Wide-Range Tuning and Enhancement of Organic Long-Persistent Luminescence Using Emitter Dopants. *Adv. Mater.* **30**, 1800365 (2018).

23. Lin Z, Kabe R, Wang K, Adachi C. Influence of energy gap between charge-transfer and locally excited states on organic long persistence luminescence. *Nat. Commun.* **11**, 191 (2020).

24. Nishimura N, Lin Z, Jinnai K, Kabe R, Adachi C. Many Exciplex Systems Exhibit Organic Long-Persistent Luminescence. *Adv. Funct. Mater.* **30**, 2000795 (2020).

25. Lin Z, Kabe R, Adachi C. Orange Organic Long-persistent Luminescence from an Electron Donor/Acceptor Binary System. *Chem. Lett.* **49**, 203-206 (2020).

26. Jinnai K, Kabe R, Lin Z, Adachi C. Organic long-persistent luminescence stimulated by visible light in p-type systems based on organic photoredox catalyst dopants. *Nat. Mater.* **21**, 338-344 (2022).

27. Li W*, et al.* Organic Long-Persistent Luminescence from a Thermally Activated Delayed Fluorescence Compound. *Adv. Mater.* **32**, 2003911 (2020).

28. Alam P*, et al.* Two Are Better Than One: A Design Principle for Ultralong-Persistent Luminescence of Pure Organics. *Adv. Mater.* **32**, 2001026 (2020).

29. Liang X, Zheng Y-X, Zuo J-L. Two-Photon Ionization Induced Stable White Organic Long Persistent Luminescence. *Angew. Chem. Int. Ed.* **60**, 16984-16988 (2021).

30. Alam P*, et al.* Organic Long-Persistent Luminescence from a Single-Component Aggregate. *J. Am. Chem. Soc.* **144**, 3050-3062 (2022).

31. Freund MS, Deore BA. *Self-doped conducting polymers*. John Wiley & Sons (2007).

32. Shao S, Wang L. Through-space charge transfer polymers for solution-processed organic light-emitting diodes. *Aggregate* **1**, 45-56 (2020).

33. Shao S, Hu J, Wang X, Wang L, Jing X, Wang F. Blue Thermally Activated Delayed Fluorescence Polymers with Nonconjugated Backbone and Through-Space Charge Transfer Effect. *J. Am. Chem. Soc.* **139**, 17739-17742 (2017).

34. Rungta P, Tsyalkovsky V, Huebner CF, Bandera YP, Foulger SH. Thermal aging of single-layer polymer light-emitting diodes composed of a carbazole and oxadiazole containing copolymer doped with singlet or triplet emitters. *Synth. Met.* **160**, 2486-2493 (2010).

35. Lu C-j, Li H, Xu Q-f, Xu Q-h, Lu J-m. Synthesis and Morphology of Two Carbazole–Pyrazoline-Containing Polymer Systems and Their Electrical Memory Performance. *ChemPlusChem* **80**, 1354-1362 (2015).

36. Engels C, Van Steenwinckel D, Hendrickx E, Schaerlaekens M, Persoons A, Samyn C. Efficient fully functionalized photorefractive polymethacrylates with infrared sensitivity and different spacer lengths. *J. Mater. Chem.* **12**, 951-957 (2002).

37. Wang S, Yu C, Choi M-S, Kim S-H. Synthesis and switching properties of photochromic carbazole–spironaphthoxazine copolymer. *J. Photochem. Photobiol., A* **192**, 17-22 (2007).

38. Zhang Q-j*, et al.* The Effect of Random and Block Copolymerization with Pendent Carbozole Donors and Naphthalimide Acceptors on Multilevel Memory Performance. *Chem.: Asian J.* **13**, 853-860 (2018).

39. Tsuchida A, Nakano M, Yoshida M, Yamamoto M, Wada Y. Long-lived cation radical formation of aromatic amines in poly(methyl methacrylate) matrix at room temperature by two-photon excitation. *Polym. Bull.* **20**, 297-304 (1988).

40. Deng C, Zhang L, Wang D, Tsuboi T, Zhang Q. Exciton- and Polaron-Induced Reversible Dipole Reorientation in Amorphous Organic Semiconductor Films. *Adv. Opt. Mater.* **7**, 1801644 (2019).